Noise Analysis to Guide Denoising of Scanning Electron Microscopy Images

Sheikh Shah Mohammad Motiur Rahman [ID]
Université de Franche-Comté
CNRS, Institut FEMTO-ST
F-90000 Belfort, France
sheikh.rahman@femto-st.fr

Michel Salomon [ID]
Université de Franche-Comté
CNRS, Institut FEMTO-ST
F-90000 Belfort, France
michel.salomon@femto-st.fr

Sounkalo Dembélé [ID]
Université de Franche-Comté
CNRS, Institut FEMTO-ST
F-25000 Besançon, France
sounkalo.dembele@femto-st.fr

Abstract—The paper deals with the analysis of noise in Scanning Electron Microscopy (SEM) images with respect to the dwell time, i.e. the time to acquire a pixel. Identifying the type and parameters of noise in images is crucial for denoising, as most denoising methods rely on prior knowledge of noise. Therefore, analyzing image noise is a significant undertaking and a window-wise based image segmentation of a single image has been proposed to find the smoothest region of the image. In fact, automating the identification of the flat region, noise type estimation, and statistical verification are essential aspects of this study. All the experiments were performed on a set of images obtained from a Zeiss Auriga field effect SEM and . It is shown that the noise types and levels change with respect to dwell time. The fast (dwell time 100-500 nanoseconds) and faster scan speed (dwell time less than 100 nanoseconds) changes the noise type to Gamma distribution, while for the slow one (few microseconds or more than 500 nanoseconds) it follows a Gaussian distribution. Moreover, the level of the noise are subject to higher values with fast and very fast scan speeds. The study suggests that utilizing its findings can establish a basis for prior knowledge in deep learning denoisers, which can assist in guiding the process of SEM image denoising.

Index Terms—Scanning Electron Microscopy (SEM), Noise Analysis, Image Processing, Image Denoising

I. Introduction

The term "noise" in the context of a scanning electron microscope (SEM) refers to the random variations that can be noticed in the signal coming from a specific pixel in an image, even when the incident beam, the sample, and the recording environment are kept constant.This noise is a result of the stochastic nature of electron production from the gun and electron interactions with the specimen observed, which makes each electron behaves differently. The noise is typically assumed to have Gaussian statistics, because of the central limit theorem [1]. It is vital to evaluate this assumption since noise has a major impact on electron-beam tool's expected performance, particularly in applications like flaw identification during semiconductor manufacture. There is growing interest in mimicking SEM images for a variety of reasons, and the requirement to include realistic noise in such circumstances also highlights the issue of the precise form of the noise [2].

Despite the fact that image denoising has been studied for a long time and extremely promising denoising results have been obtained, practically almost all of the current denoisers rely on prior knowledge about the noise, such as its variance or standard deviation. Relevant studies show that under the condition of inaccurate noise parameters, the performance of state-of-the-art denoising algorithms can drop precipitously. An accurate noise parameters estimation is crucial for image processing/analysis algorithms [3]. In this paper, our goal is to present a algorithmic analysis on different SEM images, which could help us identify better parameters to perform denoising.

Noise in an image can either be additive or multiplicative. However, multiplicative noise can processed as additive when considering logarithm space. In the first case noise signal $N_{(x,y)}$ is added to the original signal $I_{original(x,y)}$ to create the corrupted noisy signal $I_{noisy(x,y)}$:

$$I_{noisy(x,y)} = I_{original(x,y)} + N_{(x,y)},$$

where (x,y) is the position of pixel.

Identifying the characteristics of final image noise is a prerequisite for estimating image quality [4], [5]. Sources of noise in digital photographic images can be environmental influences on the image sensor, low light conditions and a warm sensor, scanner dust particles and the interference with the transmission channel. However, in a SEM, primary emission, secondary emission, scintillator, photocathode, and photomultiplier are the five causes of noise [5], [6]. Thus, we will focus on the analysis of noise types and noise levels with different scanning electron microscope settings. The main focus of this study is to investigate the level of noise in SEM images concerning the dwell time, which is the time required to acquire a pixel and determines the scanning speed.

In sum up, the main objective of this study is to check whether there is any change in noise type with respect to the scan speed (or equivalently, the dwell time).

We used the Zeiss Auriga FE SEM microscope to collect sample images, in which scan speeds are represented by dwell times. We considered acquisition dwell times of 10 ms (microseconds), 2 ms, 510 ns (nanoseconds), 280 ns and 70 ns for one set of samples. A dwell time of more than 510 ns is said to be slow, from 510 ns to 100 ns as fast, less than or equal to 100 ns as faster. In the literature, [2] presents a manual

process of noise type estimation from SEM where it is most often found Gaussian and sometimes flattened. However, we found that the noise type changed from Gaussian to Gamma with respect to the scan speed, with also a few samples for which the noise found is neither exactly Gaussian nor Gamma but close to Gamma. In fact, we wanted to have an automated process to identify the type of noise in microscopy images.

To sum up, the primary goal of this work is to consider a special case of noise types in SEM images to verify if the scan speed or dwell time has an impact or not. In the literature, most of the study cases do not take into account this setting which has major impact on noise type according to our analysis. An important part of this work is to automate the process of identifying the flat region, estimating the type of noise and proving its statistics.

The contributions of this paper are as follows.

- The idea of having Gaussian noise is not always true if we consider faster scan speed for SEM images and thus we propose an approach to identify the type of noise.
- Automation of the noise identification process with algorithmic solutions, while proving it mathematically or statistically.
- One study [7] did image segmentation for identifying the flat regions from the images. But as they did not target image segmentation, they randomly used one technique, namely K-means. We used a different technique by following the concept of image segmentation using mean shift.
- Thus, in our study, we automated the process of identifying flat regions and selecting the region of interest among them.
- To identify likely flat regions, we separated the images into multiple window sizes by applying the Cartesian product of multiple fixed ratio heights and widths.
- Finally, we evaluated the results not only on the basis of the histogram, but also statistically, showing that the scan speed or dwell time has an effect on the noise type and noise level.

The rest of the paper is presented throughout the following sections. Section II describes the background and related works. The process we performed during the analysis of the images is presented in Section III. Section IV describes in detail the comparative results and findings. Finally, Section V concludes the paper with possible future work.

II. BACKGROUND AND RELATED WORKS

The most studied type of noise in imaging is Gaussian, whereas SEM can have different noise depending on the settings especially dwell time. Dwell time is the time the electron beam remains in each site to interact with surface atoms of sample. It defines the time to acquire a pixel and then the scanning speed. For the Zeiss Auriga FE SEM, the correspondences between scan speed and dwell time are given in Table I. In this study, we focus on noise analysis from the perspective of different scan speeds.

TABLE I
EXAMPLE OF ZEISS AURIGA SEM CONFIGURATIONS

Scan Speed	Dwell time
8	10 microseconds
5	2 microseconds
3	510 nanoseconds
2	280 nanoseconds
1	70 nanoseconds

A model proposed by [6] divides the SEM signal path into five stages and each stage is assumed to be Poisson distributed. We found that it really depends on the configuration and, more importantly, on scan speed. With a reduced speed scan, the image may be better, but the samples maybe damaged because of the high level of energy received per site. We consider a fast scan speed that is subjected to noise. To acquire a high quality image by performing denoising, it is crucial to analyze the noise measurements so that the SEM images can be distinguishable from other optical [8] and microscopy (fluorescence [9], [10], transmission [11], cryo [12] and so on) images.

A single image or a set of images can be used to estimate noise. Noise estimation from multiple images has overestimation problems [13]. A common estimation method is built on the mean absolute deviation (MAD) [14]. According to [15], the slope of the smooth or low-textured region is used to estimate the signal-dependent noise level for each intensity interval. Three methods to estimate noise levels based on training samples and (Laplacian) statistics of actual images are proposed in [16]. There is a piecewise smooth images model [7] that appeared first time in computer vision literature by [17] and briefly elaborated by [18]. In [7] the authors used k-means cluster for the image segmentation of piecewise smooth model as their main intention was not in image segmentation. However, for image segmentation, there are mean shifting [19] (which is focused in this study during image segmentation) and graph based techniques [20].

III. METHODOLOGY

In this study a piecewise smooth region (Region of Interest - ROI) based approach was followed. The segmentation task is performed with mean shifting [19] the ROI to more intensity (higher mean) regions. The mean shifting used is a modified version developed specifically for this study.

A. Image Grid Generation

Image grid generation is performed by generating a fixed window sized grid of the image according to Algorithm 1. This process starts by dividing a single image into multiple windows. The window size is selected by establishing a possible list of window sizes with which the total number of pixels is divisible. From the list of window sizes, the window size that falls within the middle index (not too high, not too low) is selected as the dimension (height, width) of the pieces of the smoothed region (ROI). After splitting the image, we obtain a grid of small ROI pieces. From this grid, we identify

the positions of these ROIs using the left, right, top and bottom positions. In this phase, the mean of the pixel values of each ROI will also be calculated to perform the next step of the image segmentation process based on the shift of the mean.

B. Target ROI Extraction

We calculate and pre-select multiple ROIs from the generated tiles - based on the maximum intensity of the pixels using Algorithm 2. From the values provided by Algorithm 1, we select a list of 15 higher density ROIs based on the ROI with mean values between medium to maximum. It is observed during this experiment that the 15-values condition was ideal for our experiments, which may change depending on possible smoother areas in the experimental image. To determine the appropriate tile size, a range of square dimensions was selected by dividing the total pixels into values ranging from 32 to 72 with a 2-pixel interval. Values with a modulus of 0 were considered potential tile size candidates. The final tile dimension was selected as the middle value in the list of dimensions. After selecting all ROIs in the previous step, visualization of the ROIs is performed for proper identification by visual assessment. The smoothest region is visually identified as the target ROI in figure 2.

C. Noise Estimation and Validation

To estimate the noise type, different types of assessment techniques were performed: the histogram based visual assessment, statistical assessments of normal distribution (Anderson-Darling [21], D'Agostino-Pearson [22], Jarque bera [23] tests) and we used fitter [24], a Python library which is used to fit probability distributions to data. To estimate the parameters of many types of distribution, including continuous and discrete distributions, fitter provides a straightforward and understandable interface. With fitter, we can quickly fit a wide range of distributions to our data and compare the fit of various distributions to select the one that best fits the data. It computes results by validating them based on residual sum of squares (RSS), which is also known as sum of squared estimate of errors (SSE), Akaike information criterion (AIC), computing Kullback-Leibler divergence (KLD), Kolmogorov–Smirnov (KS) test and other statistical tests.

In this work we considered the residual sum of squares (RSS) and KS test. Residual sum of squares in statistics refers to deviations expected from actual empirical data values. The Kolmogorov-Smirnov test, which can be used to compare two samples or a sample with a reference probability distribution, is a nonparametric statistical test for the equivalence of continuous, one-dimensional probability distributions. The categorization of the dwell time (or scan speed) was performed with the intention of performing experiments from a low scan speed to a faster speed to study whether there are changes with respect to speed.

IV. RESULTS AND DISCUSSION

From the experiments, one of the smoothest area is visually selected from the list of candidates to be the target ROI. Two

Inputs: Image name, source, target
Outputs: Position (left,up,right,down) lists of each divided windows with mean values of the image pixels

$h \leftarrow image\_height, w \leftarrow image\_width$;
/* Total pixels   */
$T_p \leftarrow (h * w)$;
/* Possible window sizes   */
$dim \leftarrow []$;
for $range \leftarrow 32$ **to** 72 *by* 2 **do**
  if T_p mod $range$ *is 0* **then**
  | $dim \leftarrow range$
  end
end
$selected\_dim \leftarrow 0$;
if $len(dim)$ *is greater 0* **then**
  | $selected\_dim \leftarrow dim[int(len(dim)/2)]$;
end
/* Grid as Cartesian product (set of height and weight)   */
$H, W \leftarrow \{\}$;
for $H \leftarrow 0$ **to** $h - (h$ mod $selected\_dim)$ *by* $selected\_dim$ **do**
  | $H \leftarrow h$;
end
for $W \leftarrow 0$ **to** $w - (w$ mod $selected\_dim)$ *by* $selected\_dim$ **do**
  | $H \leftarrow w$;
end
$grid \leftarrow H \times W$;
/* ROIs positions and means   */
$left, upper, right, lower, mean \leftarrow []$;
for $i, j \leftarrow grid$ **do**
  | $box \leftarrow (j, i, j + selected\_dim, i + selected\_dim)$;
  | $left \leftarrow j$;
  | $upper \leftarrow i$;
  | $right \leftarrow j + selected\_dim$;
  | $lower \leftarrow i + selected\_dim$;
  | $mean \leftarrow mean(img.crop(box))$;
  | $img.crop(box).save(out)$;
end
$return \leftarrow left, upper, right, lower, mean$;

Algorithm 1: Square tile or grid generation

examples of such a ROI is shown in Figure 2 and Figure 3. To analyze the noise estimate, a histogram calculation, shown in Figure 4, was first performed. From Figure 4, the initial assumption was that scan speeds 8 through 2 (see the histograms (b) to (e) in Figure 4) lead to normal distributions (Gaussian statistics) and the distribution of scan speed 1 to not normal distribution. Then, to validate this assumption, some statistical approaches were applied on the pixel values of the ROI along with fitter test with respect to found model. The statistical Anderson-Darling Test, D'Agostino-Pearson Omnibus Test and Jarque bera Test were used for this purpose: H0,
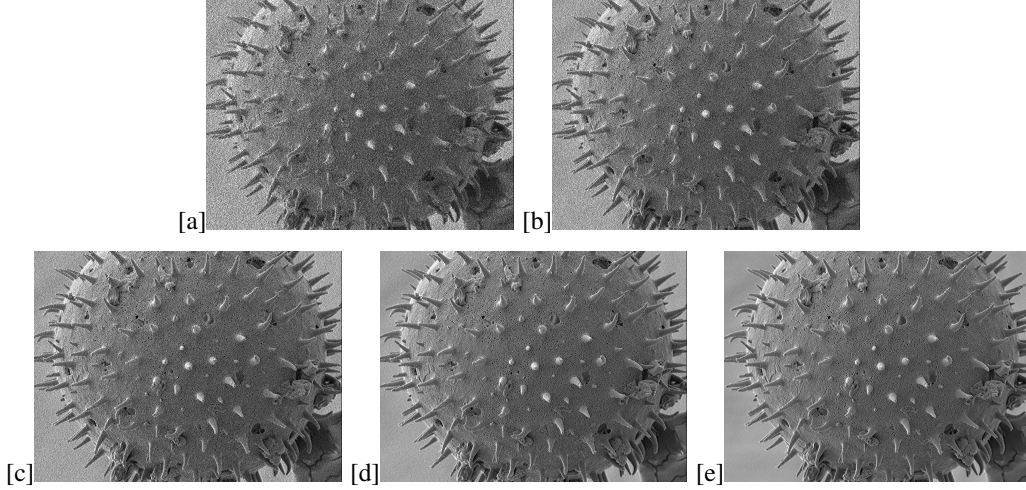
Fig. 1. Samples for speed 1 (a), speed 2 (b), speed 3 (c), speed 5 (d) and speed 8 (e).

Inputs: output of Algo. 1 (left,upper,right,lower,mean)
Outputs: Selected ROIs (lefts,uppers,rights,lowers)
$mid\_mean = int((min(mean) + max(mean))/2);$
$max\_mean = int(max(mean));$
$pre\_select \leftarrow [];$
for M **in** $mean$ **do**
    if $mid\_mean < M < max\_mean$ **then**
        $pre\_select \leftarrow M;$
    end
end
$selected\_values \leftarrow [];$
while $|pre\_select| \leq 15$ **do**
    for X **in** pre_select **do**
        if $mean(pre\_select) < X < max(pre\_select)$
        then
            $selected\_values \leftarrow X;$
        end
    end
    $pre\_select \leftarrow selected\_values$
end
$l\_select , u\_select, r\_select, low\_select \leftarrow [];$
for i **in** $selected\_values$ **do**
    $index \leftarrow mean.index(i);$
    $l\_select \leftarrow left[index];$
    $u\_select \leftarrow upper[index];$
    $r\_select \leftarrow right[index];$
    $low\_select \leftarrow lower[index];$
end
$return \leftarrow l\_select, u\_select, r\_select, low\_select;$
    Algorithm 2: Pre-selection of ROI candidates

distribution is normal and H1, it is not normal. If the scores of all tests are more than the p-value of 0.05 (significance level) than H0 is satisfied otherwise H1. The results of the statistical tests are described in Table II. Note that there are conflicting statements from researchers about the p-value which can be 0.001 to 0.05. Thus, the Anderson-Darling Test has a dynamic p-value selection set to make the evaluation more valid.

From a statistical point of view, the results do not match the initial assumptions of the visual evaluations based on the histograms. It is clear that slow (dwell time greater than 510 ns) and fast (dwell time between 510 ns and 100 ns) scan speeds exhibit Gaussian-like distributions. However, for faster speeds (less than 100 ns), the noise is not Gaussian but, from the histogram, resembles a Poisson-like distribution. In fact, some histograms are not clearly Gaussian but look like a Gaussian distribution. Therefore, a fitter test was performed to further validate the distribution by fitting it to various distributions. The fitter test of the pixel values in the ROI, shown in Table III, shows that the noise in the fast and faster scan rates follows a Gamma distribution or a special case of Gamma.

We performed the same experiments with a different set of samples collected from a different SEM (Figure refspdus). We obtained similar results, but for a few rare samples we found in the fitter test that the distribution could be a special case of Gamma, i.e. Chi-squared and Rayleigh, or sometimes Lognormal as well.

Indeed, the ROI was tested with about 10 types of common distributions and sometimes the results of the Gamma and Chi-squared tests have a similar sum of residual squares (RSS) as shown in Table IV. In fact, the misclassification of the Gamma distribution as normal in the statistical test may be due to the selection of an inappropriate p-value threshold. In addition, it is essential to differentiate these two distributions because of their relationship to the zero mean. If the shape value increases in the Gamma distribution, it tends to become a Gaussian one, which can lead to confusion in the statistical test.
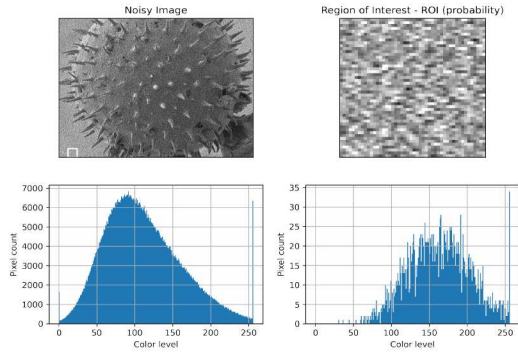
Fig. 2. Selected ROI for scan speed 1.

The conclusions that the faster and faster scan rate tends to be a Gamma distribution or a family of Gamma distributions also fit the theory. For example, one study showed that at each step of the SEM, fish events were obtained [25], based on which another study performed a classification of the noise estimate in [26].In fact, a generic kind of statistical distribution known as a Gamma distribution, which is connected to the Beta distribution, naturally develops in systems where the waiting intervals between Poisson distributed events are significant [27]. Thus, in summary, a SEM provides Poisson distributed events [25] and Gamma appears in Poisson distributed events [27], which proves the validity of our findings theoretically too.
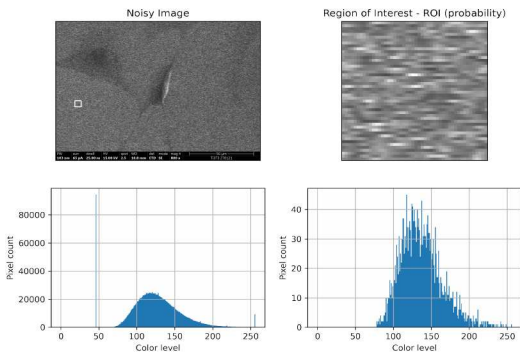
Fig. 3. Selected ROI for dwell time 25 ns.

TABLE II
COMPARISON OF THE RESULTS OF THE STATISTICAL TESTS

Dwell time	Anderson-Darling	D'Agostino-Pearson	Jarque bera
10 ms	Gaussian	Gaussian	Gaussian
2 ms	Gaussian	Gaussian	Gaussian
510 ns	Gaussian	Gaussian	Not Gaussian
280 ns	Not Gaussian	Not Gaussian	Not Gaussian
70 ns	Not Gaussian	Not Gaussian	Not Gaussian

TABLE III
COMPARISON OF THE RESULTS OF THE FITTING DISTRIBUTIONS (SEM1)

Dwell time	Type	RSS / SSE	KS-statistic
70 ns	gamma	0.000358	0.021746
	norm	0.000359	0.022148
	chi2	0.000364	0.020554
280 ns	gamma	0.000418	0.013230
	norm	0.000418	0.013132
	rayleigh	0.000665	0.090348
510 ns	norm	0.000791	0.015321
	cauchy	0.001257	0.078619
	rayleigh	0.001481	0.140688
2 ms	norm	0.001535	0.023570
	cauchy	0.002834	0.073744
	rayleigh	0.004744	0.178042
10 ms	norm	0.306655	0.048039
	gamma	0.306665	0.0482287
	lognorm	0.306808	0.051615

TABLE IV
COMPARISON OF THE RESULTS OF THE FITTING DISTRIBUTIONS (SEM2)

Dwell time	Type	RSS / SSE	KS-statistic
25 ns	gamma	0.000675	0.014127
	chi2	0.000675	0.014127
	lognorm	0.000678	0.015412
50 ns	chi2	0.000536	0.019112
	gamma	0.000536	0.019112
	lognorm	0.000540	0.020630
300 ns	gamma	0.000411	0.021313
	norm	0.000441	0.033449
	rayleigh	0.000604	0.078607
5 ms	norm	0.146091	0.042473
	gamma	0.146151	0.043740
	lognorm	0.14153	0.043851

V. CONCLUSION AND FUTURE WORK

Noise analysis and estimation is a crucial subject of study because it is important to have prior knowledge to denoise any noisy image. This is particularly the case for SEM where noise is dependent of the scanning speed. Therefore a single image noise analysis with SEM with multiple scan speed has been briefly explored in this study. The results of the analysis have been validated by assessments based on statistics of the smoothest region. It was found that the noise in the SEM images has different behaviors depending on the scanning speed. More precisely, scan speeds above 510 nanoseconds produce images with Gaussian noise statistics while relatively fast speed 100-510 nanoseconds and faster scan speeds below 100 nanoseconds produce a Gamma-like noise distribution. Furthermore, it was also noticed that the noise level was higher in relation to the slow-fast-faster scan speed. We will continue this work by developing a deep learning based classifier to perform automatic noise estimation. In addition, an experiment with state-of-the-art denoisers will be performed with the prior information found in this study.
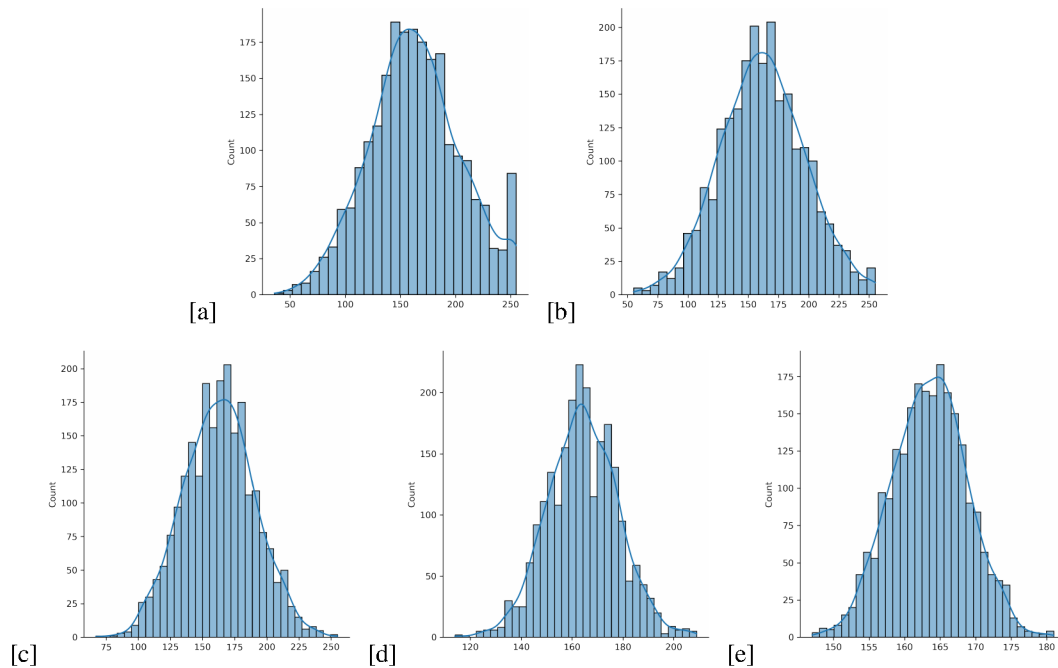
Fig. 4. Histograms of the smoothest ROI for speed 1 (a), speed 2 (b), speed 3 (c), speed 5 (d) and speed 8 (e).

REFERENCES

[1] L. Le Cam, "The central limit theorem around 1935," *Statistical science*, pp. 78–91, 1986.

[2] M. S. Prasad and D. C. Joy, "Is SEM noise gaussian?" *Microscopy and Microanalysis*, vol. 9, no. S02, pp. 982–983, 2003.

[3] C. Tang, X. Yang, and G. Zhai, "Noise estimation of natural images via statistical analysis and noise injection," *IEEE Transactions on Circuits and Systems for Video Technology*, vol. 25, no. 8, pp. 1283–1294, 2014.

[4] L. Vijaysinh, "A Guide to Different Types of Noises and Image Denoising Methods," https://analyticsindiamag.com, 2021.

[5] N. Marturi, S. Dembélé, and N. Piat, "Scanning electron microscope image signal-to-noise ratio monitoring for micro-nanomanipulation," *Scanning: The Journal of Scanning Microscopies*, vol. 36, no. 4, pp. 419–429, 2014.

[6] F. Timischl, M. Date, and S. Nemoto, "A statistical model of signal–noise in scanning electron microscopy," *Scanning*, vol. 34, no. 3, pp. 137–144, 2012.

[7] C. Liu, R. Szeliski, S. B. Kang, C. L. Zitnick, and W. T. Freeman, "Automatic estimation and removal of noise from a single image," *IEEE transactions on pattern analysis and machine intelligence*, vol. 30, no. 2, pp. 299–314, 2007.

[8] Q. Lu, C. Liu, W. Feng, Q. Xiao, and X. Wang, "Deep learning optical image denoising research based on principal component estimation," *Applied Optics*, vol. 61, no. 15, pp. 4412–4420, 2022.

[9] V. Mannam, Y. Zhang, Y. Zhu, E. Nichols, Q. Wang, V. Sundaresan, S. Zhang, C. Smith, P. W. Bohn, and S. S. Howard, "Real-time image denoising of mixed poisson–gaussian noise in fluorescence microscopy images using ImageJ," *Optica*, vol. 9, no. 4, pp. 335–345, 2022.

[10] B. Mandracchia, X. Hua, C. Guo, J. Son, T. Urner, and S. Jia, "Fast and accurate sCMOS noise correction for fluorescence microscopy," *Nature communications*, vol. 11, no. 1, pp. 1–12, 2020.

[11] T. Tasdizen, R. Whitaker, R. Marc, and B. Jones, "Enhancement of cell boundaries in transmission electron microscopy images," in *IEEE International Conference on Image Processing 2005*, vol. 2.   IEEE, 2005, pp. II–129.

[12] F. J. Sigworth, "Principles of cryo-em single-particle image processing," *Microscopy*, vol. 65, no. 1, pp. 57–67, 2016.

[13] G. E. Healey and R. Kondepudy, "Radiometric CCD camera calibration and noise estimation," *IEEE Transactions on Pattern Analysis and Machine Intelligence*, vol. 16, no. 3, pp. 267–276, 1994.

[14] D. L. Donoho, "De-noising by soft-thresholding: Ieee transactions on information theory," 1995.

[15] W. Förstner, "Image preprocessing for feature extraction in digital intensity, color and range images," in *Geomatic method for the analysis of data in the earth sciences*.   Springer, 2000, pp. 165–189.

[16] A. De Stefano, P. R. White, and W. B. Collis, "Training methods for image noise level estimation on wavelet components," *EURASIP Journal on Advances in Signal Processing*, vol. 2004, no. 16, pp. 1–8, 2004.

[17] M. Tappen, W. Freeman, and E. Adelson, "Recovering intrinsic images from a single image," *Advances in neural information processing systems*, vol. 15, 2002.

[18] A. Blake and A. Zisserman, *Visual reconstruction*.   MIT press, 1987.

[19] D. Comaniciu and P. Meer, "Mean shift: A robust approach toward feature space analysis," *IEEE Transactions on pattern analysis and machine intelligence*, vol. 24, no. 5, pp. 603–619, 2002.

[20] P. F. Felzenszwalb and D. P. Huttenlocher, "Efficient graph-based image segmentation," *International journal of computer vision*, vol. 59, no. 2, pp. 167–181, 2004.

[21] M. A. Stephens, "Edf statistics for goodness of fit and some comparisons," *Journal of the American statistical Association*, vol. 69, no. 347, pp. 730–737, 1974.

[22] R. DIAgostino, "An omnibus test of normality for moderate and large sample sizes," *Biometrika*, vol. 58, no. 34, pp. 1–348, 1971.

[23] C. M. Jarque and A. K. Bera, "Efficient tests for normality, homoscedasticity and serial independence of regression residuals," *Economics letters*, vol. 6, no. 3, pp. 255–259, 1980.

[24] T. Cokelaer, A. Kravchenko, lahdjirayhan, msat59, A. Varma, B. L, C. E. Stringari, C. Brueffer, E. Broda, E. Pruesse, K. Singaravelan, Z. Li, mark padgham, and negodfre, "cokelaer/fitter: v1.5.2," Jan. 2023. [Online]. Available: https://doi.org/10.5281/zenodo.7497983

[25] F. Timischl, M. Date, and S. Nemoto, "A statistical model of signal–noise in scanning electron microscopy," *Scanning*, vol. 34, no. 3, pp. 137–144, 2012.

[26] S. S. M. M. Rahman, M. Salomon, and S. Dembele, "Machine learning aided classification of noise distribution in scanning electron microscopy images," in *2023 3nd International Conference on Computer, Control and Robotics (ICCCR)*.   In press, IEEE.

[27] E. W. Weisstein, "Gamma Distribution. From MathWorld–A Wolfram Web Resource. ," https://mathworld.wolfram.com/GammaDistribution.html.